arXiv:2410.14791v1 [hep-ph] 18 Oct 2024

Axion effects on gamma-ray spectral irregularities. II: EBL absorption models

Hai-Jun Li[a], Wei Chao[b], Xiu-Hui Tan[a], and Yu-Feng Zhou[a,c,d,e]

[a]*Key Laboratory of Theoretical Physics, Institute of Theoretical Physics, Chinese Academy of Sciences, Beijing 100190, China*

[b]*Center for Advanced Quantum Studies, Department of Physics, Beijing Normal University, Beijing 100875, China*

[c]*School of Physical Sciences, University of Chinese Academy of Sciences, Beijing 100049, China*

[d]*School of Fundamental Physics and Mathematical Sciences, Hangzhou Institute for Advanced Study, UCAS, Hangzhou 310024, China*

[e]*International Centre for Theoretical Physics Asia-Pacific, Beijing/Hangzhou, China*

E-mail: lihaijun@itp.ac.cn, chaowei@bnu.edu.cn, tanxh@itp.ac.cn, yfzhou@itp.ac.cn

ABSTRACT: In this study, we explore how the extragalactic background light (EBL) absorption effect influences the photon to axionlike particle (ALP) conversions from the very-high-energy gamma-ray spectral irregularities. For our analysis, we select two well-known BL Lac blazars: Markarian 421 and Markarian 501 with their low and well-defined redshifts $z_0 = 0.031$ and 0.034, respectively. Their gamma-ray data are recently measured by Fermi-LAT and HAWC with the 1038 days of exposure from 2015 June to 2018 July. We first discuss the EBL absorption effect on the gamma-ray spectral energy distributions by using three common EBL spectral models: Franceschini-08, Finke-10, and Gilmore-12. Then we consider the photon-ALP conversions in the astrophysical magnetic fields. Under the ALP assumption with the parameter space of $\{m_a, g_{a\gamma}\}$, we calculate the best-fit chi-square distribution of the EBL models and define a new delta chi-square χ_d^2 to quantify the chi-square difference. Our results show that the impact from these different EBL spectral models are non-dominated at the low-redshift gamma-ray axionscope.

KEYWORDS: axions, active galactic nuclei, extragalactic background light, gamma ray theory

Contents

1   Introduction

Axions are excellent candidates for new physics. The QCD axion was originally introduced by the Peccei-Quinn (PQ) mechanism to dynamically solve the strong CP problem in the Standard Model (SM) [1–4], meanwhile, it also provides a natural source for cold dark matter (DM) through the misalignment mechanism [5–7]. On the other hand, the axionlike particle (ALP), predicted by a variety of theories [8, 9], is also the attractive DM candidate [10–12], but does not have to solve the strong CP problem. The axion can couple to the photon with the effective Lagrangian

$$
\begin{aligned}
\mathcal{L} &= \frac{1}{2}\partial_\mu a \partial^\mu a - \frac{1}{2}m_a^2 a^2 - \frac{1}{4}g_{a\gamma} a F_{\mu\nu}\tilde{F}^{\mu\nu} \\
&= \frac{1}{2}\partial_\mu a \partial^\mu a - \frac{1}{2}m_a^2 a^2 + g_{a\gamma} a \mathbf{E}\cdot\mathbf{B}\,,
\end{aligned}
\tag{1.1}
$$

where a and m_a donate the axion field and axion mass, respectively, $g_{a\gamma}$ is the axion-photon coupling constant, $F_{\mu\nu}$ ($\tilde{F}^{\mu\nu}$) is the (dual) electromagnetic field tensor, $\mathbf{E}$ and $\mathbf{B}$ are the local electric and magnetic field vectors, respectively. In the QCD axion scenario, the axion mass m_a and coupling $g_{a\gamma}$ are interrelated, whereas in the ALP scenario, they are considered independent parameters. Therefore, the ALP has a much wider $\{m_a, g_{a\gamma}\}$ parameter space than the QCD axion. See ref. [13] for the latest ALP-photon limits.

The coupling between the ALPs and the very-high-energy (VHE; $\sim \mathcal{O}(100)\,\mathrm{GeV}$) photons in the astrophysical magnetic fields could lead to some detectable signals, such as a reduced TeV opacity of the Universe [14–16]. The VHE gamma-rays from the extragalactic

Source	redshift	Gal.Long. (deg)	Gal.Lat. (deg)
Markarian 421	0.031	179.88	65.01
Markarian 501	0.034	63.60	38.86

Table 1. The redshift and position informations of the sources Markarian 421 and Markarian 501. See also http://tevcat2.uchicago.edu for more details.

sources, such as blazars, are mainly affected by the extragalactic background light (EBL) absorption effect due to the electron-positron pair production process

$$\gamma_{\text{TeV}} + \gamma_{\text{EBL}} \to e^- + e^+ \,, \tag{1.2}$$

where γ_{TeV} and γ_{EBL} are the VHE photons and background photons, respectively. By taking into account the photon-ALP conversions and back-conversions in the simulated astrophysical magnetic fields, the EBL absorption effect can be mitigated, resulting in the Universe that is potentially more transparent than previously thought solely based on the EBL absorption [17, 18]. Furthermore, it also offers a natural mechanism for constraining ALP properties, and many similar studies have recently been conducted within this axionscope scenario [19–49].

Previous studies show that the source magnetic field parameter, such as the strength of the core magnetic field, has the most significant influence on the limits of ALP properties [29, 31]. Moreover, the uncertainty in the source redshift can also have an impact, as both underestimated and overestimated redshift values can affect the ALP limits [50]. In principle, different EBL spectral models bring different behaviors, and it is worth investigating them quantitatively, even though their outcomes can be naively predicted.

In this work, we explore the impact of the EBL absorption effect on photon-ALP conversions from the VHE gamma-ray spectral irregularities. In this regard, the gamma-ray source should be selected with a relatively certain redshift. For our purpose, we select these two well-known BL Lac blazars: Markarian 421 (with the redshift $z_0 = 0.031$) and Markarian 501 (with the redshift $z_0 = 0.034$). See also table 1 for their position informations. Here we use the VHE gamma-ray data of Markarian 421 and Markarian 501 measured by Fermi-LAT and HAWC with the 1038 days of exposure from 2015 June to 2018 July [51][1]. We first discuss the EBL absorption effect on the gamma-ray spectral energy distributions (SEDs) with the three common EBL spectral models. Then we consider the photon-ALP conversions in the astrophysical magnetic fields. The best-fit chi-square distribution of these EBL models under the ALP assumption in the ALP parameter $\{m_a, g_{a\gamma}\}$ plane are given, showing a similar distribution. For comparison, we define a new delta chi-square χ_d^2 to quantify the chi-square difference. The distribution of χ_d^2 and the gamma-ray SEDs corresponding to χ_d^2 are also shown. Finally, we find that there is only a minor influence from the different EBL models at the low-redshift gamma-ray axionscope.

---

[1]This data of Markarian 421 was recently investigated in ref. [52] to constrain the axion-photon coupling, showing a stringent upper limit in the axion mass region $[1.0 \times 10^{-9}\,\text{eV} \lesssim m_a \lesssim 1.0 \times 10^{-8}\,\text{eV}]$. However, in this work, we do not intend to set any limits on axion, but rather focus on the EBL absorption effect using different EBL spectral models.

The rest of this paper is structured as follows. In section 2, we introduce the EBL absorption effect on the VHE gamma-ray propagation and show the gamma-ray data of the selected blazars. In section 3, we discuss the photon-ALP conversions in the astrophysical magnetic fields. The analysis and results under the ALP assumption are given in section 4. Finally, the conclusion is given in section 5.

2 The gamma-ray SEDs under the null hypothesis

In this section, we first introduce the EBL absorption effect on the VHE gamma-ray propagation, then we show the gamma-ray SEDs of the selected BL Lac blazars Markarian 421 and Markarian 501.

2.1 EBL absorption effect

In general, due to eq. (1.2) the main effect on the VHE photons (with the high energy E) from the extragalactic space is the EBL photons (with the low energy ω) absorption effect with the absorption factor $e^{-\tau}$

$$\Phi(E) = e^{-\tau}\Phi_{\text{int}}(E) \,, \tag{2.1}$$

where $\Phi(E)$ is the gamma-ray expected spectrum, $\Phi_{\text{int}}(E)$ is the intrinsic spectrum, and τ is the optical depth. This optical depth can be described by [53]

$$\tau = c \int_0^{z_0} \frac{\mathrm{d}z}{(1+z)H(z)} \int_{E_{\text{th}}}^{\infty} \mathrm{d}\omega \frac{\mathrm{d}n(z)}{\mathrm{d}\omega} \bar{\sigma}(E, \omega, z) \,, \tag{2.2}$$

with the Hubble expansion rate

$$H(z) = H_0 \sqrt{(1+z)^2 (1+\Omega_m z) - z(2+z)\Omega_\Lambda} \,, \tag{2.3}$$

where z_0 is the source redshift, E_{th} is the threshold energy, $\bar{\sigma}(E, \omega, z)$ represents the integral pair-production cross section, $\mathrm{d}n(z)/\mathrm{d}\omega$ represents the EBL proper number density, $H_0 \simeq 67.4\,\mathrm{km\,s^{-1}\,Mpc^{-1}}$, $\Omega_m \simeq 0.315$, and $\Omega_\Lambda \simeq 0.685$ [54].

In our previous studies, we did not involve different models of the EBL spectrum. For our purpose, in this work we take the spectra of EBL from the three common models: Franceschini-08 [53], Finke-10 [55], and Gilmore-12 [56], which are shown in figure 1 with the purple, green, and yellow lines, respectively. We can see that these spectra exhibit similar distributions in the near-infrared regions, but display distinct distributions in the far-infrared regions. It is worth noting that another commonly used EBL spectral model, Dominguez-11 [57], has a similar spectral distribution to that of the Franceschini-08 model, hence we will not delve into a separate discussion on it.

2.2 The gamma-ray SEDs of Markarian 421 and Markarian 501

Here we show the gamma-ray SEDs of Markarian 421 and Markarian 501 under the null hypothesis. In this work, the used VHE gamma-ray data of Markarian 421 and Markarian 501 are recently measured by Fermi-LAT and HAWC with the 1038 days of exposure
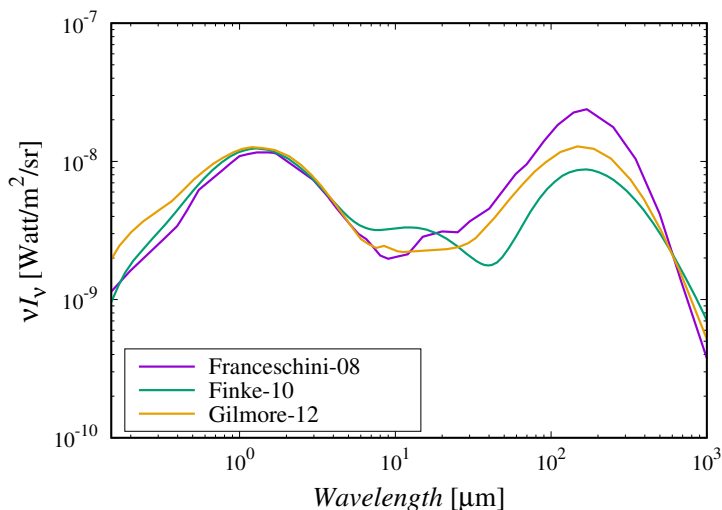
Figure 1. The EBL spectral models used in this work. The purple, green, and yellow lines represent the models Franceschini-08 [53], Finke-10 [55], and Gilmore-12 [56], respectively.

from 2015 June to 2018 July [51]. See figure 2 for the experimental data with the blue and red points, respectively.

The VHE gamma-ray intrinsic spectrum $\Phi_{\text{int}}(E)$ is selected as the power law with a super-exponential cut-off (SEPWL) model[2], which can be described by

$$\Phi_{\text{int}}(E) = N_0 \, (E/E_0)^{-\Gamma} \exp\left(-\,(E/E_c)^d\right) , \tag{2.4}$$

where N_0 is the normalization constant, Γ is the spectral index, E_c and d are free parameters, and we fix E_0 with a typical value $1\,\text{GeV}$. Then the chi-square value under the null hypothesis is given by

$$\chi^2_{\text{null}} = \sum_{i=1}^{N} \left(\frac{e^{-\tau}\Phi_{\text{int}}(E_i) - \psi(E_i)}{\delta(E_i)}\right)^2 , \tag{2.5}$$

where N is the gamma-ray spectral point number, ψ and δ are the detected flux and its uncertainty, respectively. For the experimental data of Markarian 421 and Markarian 501, we have $N = 36$ and 33, respectively.

Using the above three EBL spectral models, we show the best-fit gamma-ray SEDs of Markarian 421 and Markarian 501 under the null hypothesis in figure 2. The purple, green, and yellow lines correspond to the null hypothesis SEDs with the EBL Franceschini-08, Finke-10, and Gilmore-12, respectively. We find that their distributions are basically the same, except in the high energy $\sim \mathcal{O}(10)\,\text{TeV}$ region. This is quite understandable, as the attenuation factor is greater in these energies. In addition, the best-fit chi-square values with the different EBL spectral models are also listed in table 2.

---

[2]We have checked and found that this SEPWL intrinsic spectral model corresponds to the minimum best-fit reduced chi-square for the null hypothesis gamma-ray data of both Markarian 421 and Markarian 501 used in this work.
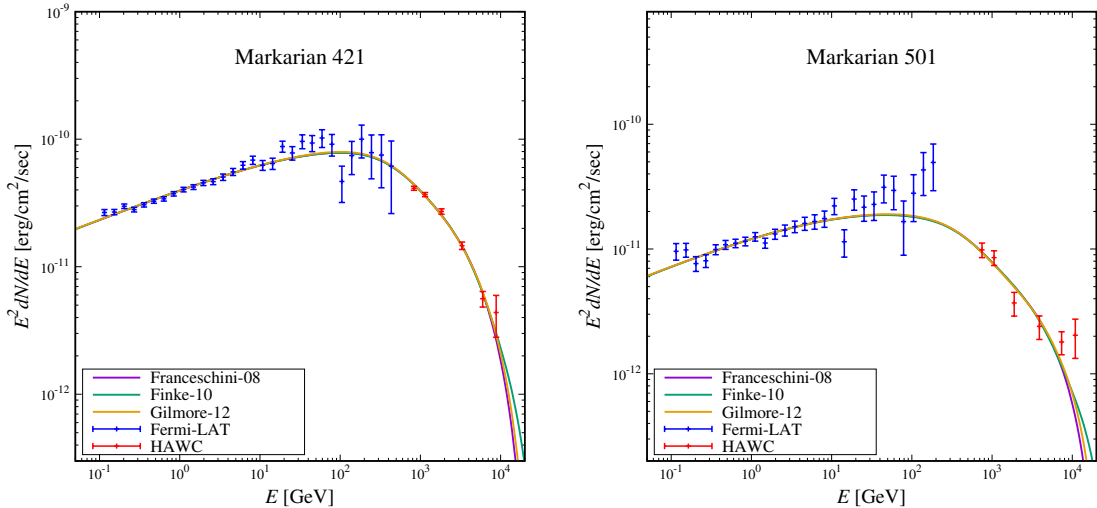
Figure 2. The best-fit null hypothesis gamma-ray SEDs of Markarian 421 (left) and Markarian 501 (right). The purple, green, and yellow lines correspond to the SEDs with the EBL spectral models Franceschini-08, Finke-10, and Gilmore-12, respectively. The blue and red points represent the experimental data of Fermi-LAT and HAWC, respectively.

Source	EBL model	χ^2_{null}	$\chi^2_{\text{null}}/\text{d.o.f.}$
Markarian 421	Franceschini-08	44.24	1.38
Markarian 421	Finke-10	43.24	1.35
Markarian 421	Gilmore-12	43.47	1.36
Markarian 501	Franceschini-08	42.06	1.45
Markarian 501	Finke-10	41.08	1.42
Markarian 501	Gilmore-12	40.28	1.39

Table 2. The best-fit null hypothesis chi-square values of Markarian 421 and Markarian 501 with the EBL spectral models Franceschini-08, Finke-10, and Gilmore-12.

3 Photon-ALP conversions in astrophysical magnetic fields

In this section, we discuss the photon-ALP conversions in the astrophysical magnetic fields. We first introduce the photon-ALP conversions in the inhomogeneous magnetic field, then we discuss the astrophysical magnetic field parameters setup.

3.1 Photon-ALP conversions in the magnetic field

Before discussing the photon-ALP conversions in the inhomogeneous astrophysical magnetic field, we have already provided the general conversions in the homogeneous magnetic field in Appendix A.

In the real astrophysical environment, the magnetic field is inhomogeneous and can be random. In order to obtain the photon-ALP conversion probability in the inhomogeneous magnetic field, the magnetic field is usually simulated with the domain-like structure and each domain can be regarded as homogeneous. In this case, the photon-ALP system can

be described by the density matrix

$$\rho(x_3) = \begin{pmatrix} A_1(x_3) \\ A_2(x_3) \\ a(x_3) \end{pmatrix} \otimes \Big(A_1(x_3), A_2(x_3), a(x_3) \Big)^*, \tag{3.1}$$

which satisfies the Von Neumann-like commutator equation

$$i\frac{\mathrm{d}\rho(x_3)}{\mathrm{d}x_3} = \rho(x_3)\mathcal{M}^\dagger(E, x_3, \theta) - \mathcal{M}(E, x_3, \theta)\rho(x_3), \tag{3.2}$$

where x_3 is the direction of propagation, A_1 and A_2 are the linear polarization amplitudes of the photon in the perpendicular directions (x_1, x_2), and a is the ALP. Notice that in a case that the transversal magnetic field B_T is not aligned along the direction of x_2 and forms a angle θ, the mixing matrix $\mathcal{M}(E, x_3)$ should be

$$\mathcal{M}(E, x_3) \to \mathcal{V}^\dagger(\theta)\mathcal{M}(E, x_3)\mathcal{V}(\theta), \tag{3.3}$$

with

$$\mathcal{V}(\theta) = \begin{pmatrix} \cos\theta & -\sin\theta & 0 \\ \sin\theta & \cos\theta & 0 \\ 0 & 0 & 1 \end{pmatrix}, \tag{3.4}$$

and we have the mixing matrix

$$\mathcal{M}(E, x_3, \theta) = \begin{pmatrix} \Delta_{11}(E, x_3) & 0 & \Delta_{a\gamma}(x_3)\sin\theta \\ 0 & \Delta_{22}(E, x_3) & \Delta_{a\gamma}(x_3)\cos\theta \\ \Delta_{a\gamma}(x_3)\sin\theta & \Delta_{a\gamma}(x_3)\cos\theta & \Delta_{aa}(E) \end{pmatrix}. \tag{3.5}$$

The Δ terms in eq. (3.5) can be found in Appendix A with the homogeneous magnetic field. The solution of eq. (3.2) can be described by

$$\rho(x_3) = \mathcal{T}(E, x_3, \theta)\rho(0)\mathcal{T}^\dagger(E, x_3, \theta), \tag{3.6}$$

where $\mathcal{T}(E, x_3, \theta)$ is the whole transport matrix of the n domains

$$\mathcal{T}(E, x_3, \theta) = \prod_{i=1}^n \mathcal{T}(E_i, x_{3,i}, \theta_i), \tag{3.7}$$

and $\rho(0)$ is the initial density matrix

$$\rho(0) = \frac{1}{2}\begin{pmatrix} 1 & 0 & 0 \\ 0 & 1 & 0 \\ 0 & 0 & 0 \end{pmatrix}. \tag{3.8}$$

Then the photon-ALP-photon conversion probability, or the final photon survival probability, can be described by

$$\mathcal{P}_{\gamma\gamma} = \mathrm{Tr}\left[(\rho_{11} + \rho_{22})\,\mathcal{T}(E, x_3, \theta)\rho(0)\mathcal{T}^\dagger(E, x_3, \theta) \right], \tag{3.9}$$

with the matrices

$$\rho_{11} = \begin{pmatrix} 1 & 0 & 0 \\ 0 & 0 & 0 \\ 0 & 0 & 0 \end{pmatrix}, \quad \rho_{22} = \begin{pmatrix} 0 & 0 & 0 \\ 0 & 1 & 0 \\ 0 & 0 & 0 \end{pmatrix}. \tag{3.10}$$

See also ref. [58] for more details in the calculation.

3.2 Astrophysical magnetic fields setup

Here we discuss the astrophysical magnetic fields setup associated the photon-ALP beam propagating from the VHE gamma-ray source region to the Earth. Generally, this process is composed of three parts: (1) the source region, (2) the extragalactic space, and (3) the Milky Way.

Firstly, for (1) the source region of the BL Lac object, the blazar jet magnetic field can be described by the poloidal and toroidal components. We consider the photon-ALP conversions in the transverse magnetic field model $B(r) = B_0(r/r_{\mathrm{VHE}})^{-1}$ with the electron density model $n_{\mathrm{el}}(r) = n_0(r/r_{\mathrm{VHE}})^{-2}$, where $r_{\mathrm{VHE}} \sim R_{\mathrm{VHE}}/\theta_{\mathrm{jet}}$ represents the distance between the VHE emission region and the central black hole of the source, R_{VHE} represents the radius of the VHE emission, θ_{jet} represents the angle between the jet axis and the line of sight, B_0 and n_0 represent the core magnetic field and electron density at the distance r_{VHE}, respectively. Since n_0 has a minimal impact on the final result, we take $n_0 = 1 \times 10^3 \, \mathrm{cm}^{-3}$ as a typical value in this work. Here we also consider the energy transformation with the Doppler factor, $\delta_{\mathrm{D}} = E_L/E_j$, where E_L and E_j represent the energy in the laboratory and co-moving frames, respectively. For the jet region $r > 1 \, \mathrm{kpc}$, the magnetic field is taken as zero. Additionally, for the host galaxy region of the source, the photon-ALP conversion effect can be totally neglected. Then for (2) the extragalactic space, we just need to consider the EBL absorption effect on the VHE gamma-rays due to the electron-positron pair-production process, see also section 2.1. Since the strength of magnetic field in the extragalactic space is small with the upper limit $\sim \mathcal{O}(1) \, \mathrm{nG}$ [59, 60], the photon-ALP conversion effect will be weak, and thus we do not consider the photon-ALP conversions in this part. Finally, in (3) the Milky Way, we should consider the photon-ALP conversions again in the Galactic magnetic field. Generally, this magnetic field can be modeled with the disk and halo components (parallel to the Galactic plane), and the so-called "X-field" component (out-of-plane) at the Galactic center [61, 62]. See also refs. [63, 64] for the latest version of this Galactic magnetic field model.

Here we list the blazar jet magnetic field model parameters B_0, R_{VHE}, θ_{jet}, r_{VHE}, and δ_{D} of Markarian 421 and Markarian 501 in table 3.

Source	B_0 (mG)	R_{VHE} (10^{17} cm)	θ_{jet} (deg)	r_{VHE} (10^{17} cm)	δ_{D}
Markarian 421	24	0.5	2.0	14.3	25
Markarian 501	20	1.0	3.0	19.1	13

Table 3. The blazar jet magnetic field model parameters of Markarian 421 and Markarian 501, which are taken from ref. [51].

4 Analysis and results

In this section, we show our analysis and results under the ALP assumption. After considering the above photon-ALP conversion effect, we can derive the final photon survival probability $\mathcal{P}_{\gamma\gamma}$, then the chi-square value under the ALP assumption is given by

$$\chi^2_{\mathrm{ALP}} = \sum_{i=1}^{N} \left(\frac{\mathcal{P}_{\gamma\gamma}\Phi_{\mathrm{int}}(E_i) - \psi(E_i)}{\delta(E_i)} \right)^2 . \tag{4.1}$$

Notice that in the calculations the EBL absorption effect in the extragalactic space is also included in the final photon survival probability. For one ALP $\{m_a, g_{a\gamma}\}$ parameter set, we can derive the best-fit χ^2_{ALP} under the ALP assumption, and also the best-fit χ^2_{ALP} distribution in the whole ALP parameter plane. By utilizing this chi-square distribution, we can obtain the $\Delta\chi^2_{\mathrm{ALP}}$ at the particular confidence level to establish the corresponding ALP bound. However, here we do not intend to set the ALP limit.

We show in figure 3 the best-fit chi-square distribution of Markarian 421 and Markarian 501 under the ALP assumption in the $\{m_a, g_{a\gamma}\}$ plane. The three EBL spectral models Franceschini-08, Finke-10, and Gilmore-12 are arranged from top to bottom. Compared with the panels of the same source, we find that there is no significant changes in the χ^2_{ALP} of the same parameter set across different EBL spectral models. In order to facilitate a clear comparison, we select two naively values of $\Delta\chi^2_{\mathrm{ALP}}$ — 46 for Markarian 421 and 50 for Markarian 501 — to illustrate in the plot. These are depicted as red contours in figure 3. Notice that these red contours are solely presented for the purpose of comparing the chi-square difference between the different EBL spectral models, thus the value of $\Delta\chi^2_{\mathrm{ALP}}$ for the same source should be assumed constant. Nonetheless, the contour distributions are largely consistent across the different EBL spectral models.

Therefore, in order to characterize the difference in chi-square between the three different EBL spectral models in this work, it is necessary to define the delta chi-square for each $\{m_a, g_{a\gamma}\}$ set

$$\begin{aligned}
\chi^2_d &= \frac{1}{6} \sum_{i=1}^{3} \sum_{j=1}^{3} (1 - \delta_{ij}) \left| \chi^2_{\mathrm{ALP},i} - \chi^2_{\mathrm{ALP},j} \right| \\
&= \frac{1}{3} \left(\left| \chi^2_{\mathrm{ALP},1} - \chi^2_{\mathrm{ALP},2} \right| + \left| \chi^2_{\mathrm{ALP},1} - \chi^2_{\mathrm{ALP},3} \right| + \left| \chi^2_{\mathrm{ALP},2} - \chi^2_{\mathrm{ALP},3} \right| \right),
\end{aligned} \tag{4.2}$$

where i and j represent the number of the three EBL models, and δ_{ij} is the Kronecker delta function

$$\delta_{ij} = \begin{cases} 1, & i = j \\ 0. & i \neq j \end{cases} \tag{4.3}$$

Notice that eq. (4.2) is only used to quantify the chi-square variation, and any significant chi-square difference between the three EBL spectral models can be reflected from this value. Figure 4 shows the distribution of this delta chi-square in the $\{m_a, g_{a\gamma}\}$ plane of Markarian 421 and Markarian 501, respectively. From this plot, we can clearly observe the

(a) Markarian 421 with Franceschini-08.

(b) Markarian 501 with Franceschini-08.

(c) Markarian 421 with Finke-10.

(d) Markarian 501 with Finke-10.

(e) Markarian 421 with Gilmore-12.

(f) Markarian 501 with Gilmore-12.
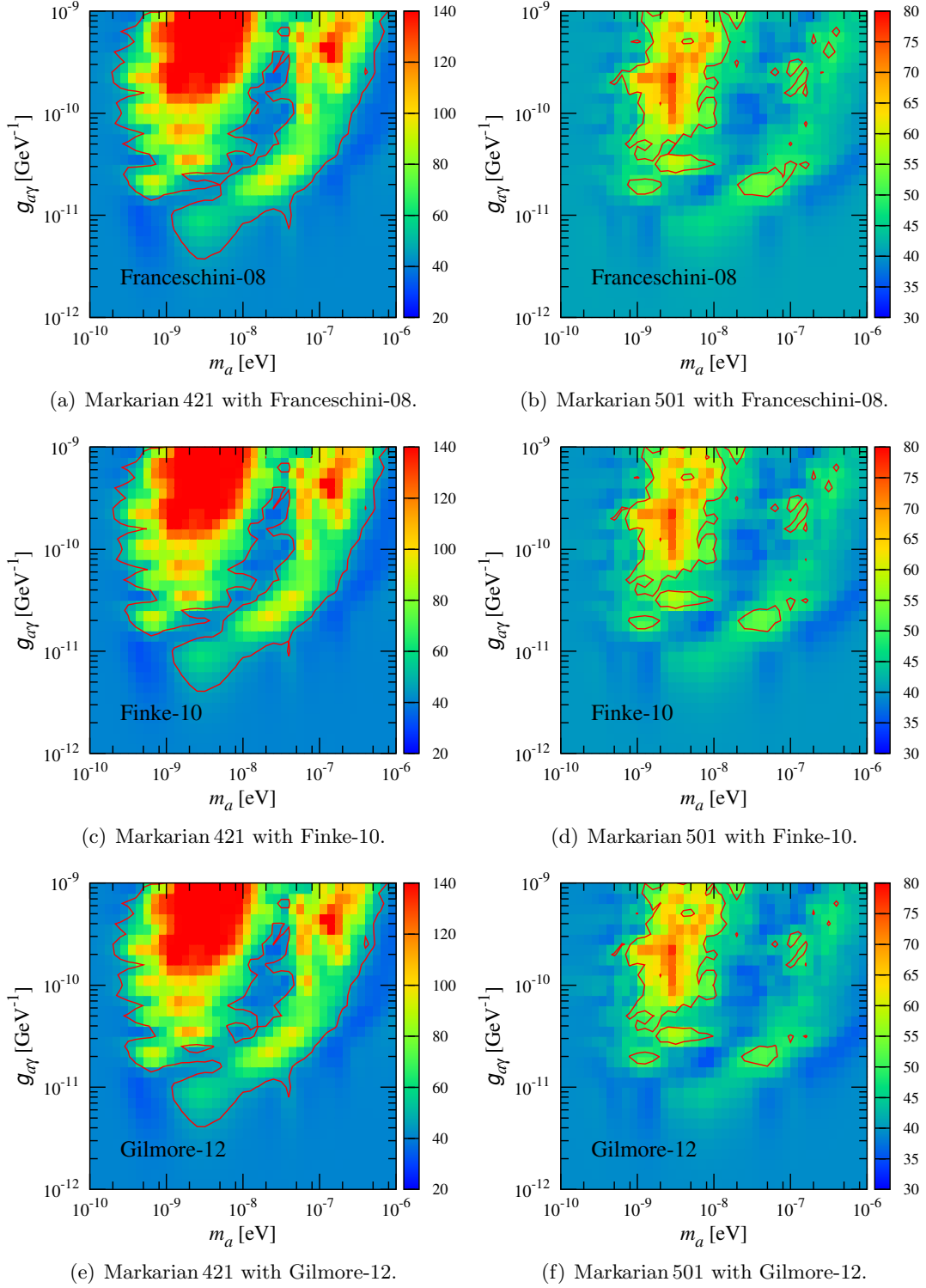
Figure 3. The best-fit ALP assumption chi-square χ^2_{ALP} distributions. The left and right panels correspond to Markarian 421 and Markarian 501, respectively. The top, middle, and bottom panels correspond to the EBL spectral models Franceschini-08, Finke-10, and Gilmore-12, respectively.

(a) Markarian 421.
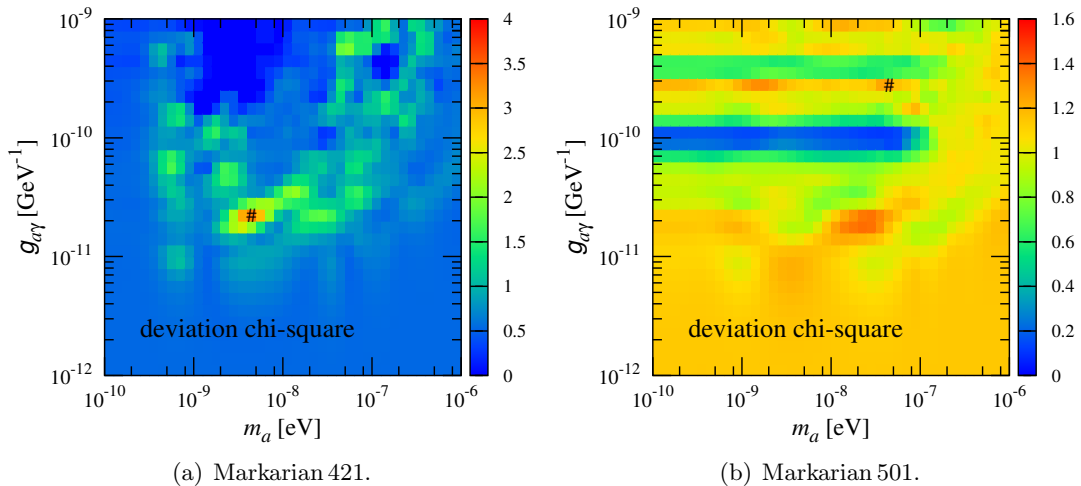
(b) Markarian 501.

Figure 4. The delta chi-square χ_d^2 distributions. The left and right panels correspond to Markarian 421 and Markarian 501, respectively. Left: the label "#" corresponds to the maximum delta chi-square $\chi_{d,\max}^2 = 3.82$ at $\{m_a \simeq 4.0 \times 10^{-9}\,\text{eV}, g_{a\gamma} \simeq 2.0 \times 10^{-11}\,\text{GeV}^{-1}\}$. Right: the label "#" corresponds to $\chi_{d,\max}^2 = 1.55$ at $\{m_a \simeq 4.0 \times 10^{-8}\,\text{eV}, g_{a\gamma} \simeq 2.5 \times 10^{-10}\,\text{GeV}^{-1}\}$.

chi-square differences and their corresponding ALP parameter points. Here the maximum delta chi-square in the $\{m_a, g_{a\gamma}\}$ plane can be defined as $\chi_{d,\max}^2$. For Markarian 421 and Markarian 501, we have $\chi_{d,\max}^2 = 3.82$ and $\chi_{d,\max}^2 = 1.55$, respectively, which are marked in figure 4 with the label "#". It is worth mentioning that certain regions in the upper left corner of figure 4 (a) correspond to $\chi_d^2 = 0$. This is a result of our decision to enhance the clarity of figure 3 by capping all chi-square values above 140 for Markarian 421, i.e., $\chi_{\text{ALP}}^2 > 140 \rightarrow \chi_{\text{ALP}}^2 = 140$. Consequently, when computing χ_d^2, these values are reduced to zero. While this adjustment is not necessary for Markarian 501.

Additionally, we also show the best-fit gamma-ray SEDs corresponding to the maximum delta chi-square $\chi_{d,\max}^2$ of Markarian 421 and Markarian 501 in figure 5. The purple, green, and yellow lines correspond to the ALP assumption SEDs with the EBL models Franceschini-08, Finke-10, and Gilmore-12, respectively. As shown in figure 2 with the null hypothesis gamma-ray SEDs, they only show the minor difference in the high energy $\sim \mathcal{O}(10)\,\text{TeV}$ region. It is anticipated that with the availability of higher energy gamma-ray data in the future, this effect will become more pronounced.

5 Conclusion

In summary, we have explored the impact of the EBL absorption effect on photon-ALP conversions from the VHE gamma-ray emitted by the BL Lac blazars. For our purpose, we select two blazars Markarian 421 and Markarian 501 for analysis. Their redshifts are measured to be $z_0 = 0.031$ and 0.034, respectively. The gamma-ray data utilized in this analysis are obtained from the recent measurements of Fermi-LAT and HAWC. We examine the impact of EBL absorption on the gamma-ray SEDs using the three commonly employed EBL spectral models: Franceschini-08, Finke-10, and Gilmore-12. Our findings reveal that
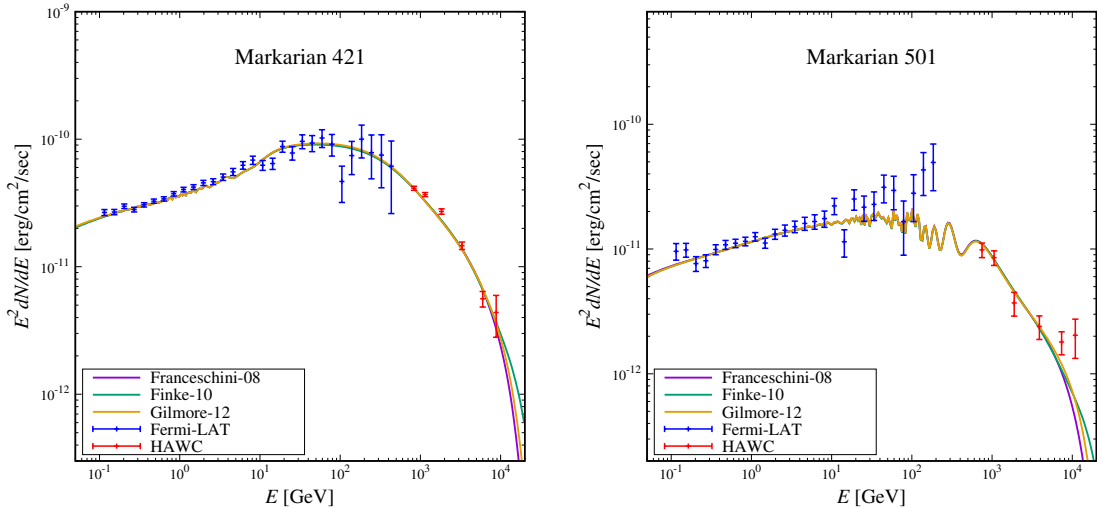
Figure 5. The best-fit ALP assumption gamma-ray SEDs corresponding to $\chi^2_{d,\mathrm{max}}$ of Markarian 421 (left) and Markarian 501 (right). The purple, green, and yellow lines correspond to the SEDs with the EBL spectral models Franceschini-08, Finke-10, and Gilmore-12, respectively.

the distributions of their SEDs are largely consistent, with notable variations only in the high energy $\sim \mathcal{O}(10)\,\mathrm{TeV}$ region.

We then delve into the analysis of photon-ALP conversions within astrophysical magnetic fields. This includes a discussion on photon-ALP conversions in both inhomogeneous magnetic fields and the astrophysical magnetic field configurations. Subsequently, we present the best-fit chi-square distribution of the various EBL models under the ALP assumption in the ALP parameter $\{m_a, g_{a\gamma}\}$ space, revealing a consistent distribution. To facilitate comparison, we introduce a delta chi-square χ^2_d to quantify the differences in chi-square values among the different EBL models, which illustrates the distribution of χ^2_d and the corresponding gamma-ray SEDs associated with χ^2_d. In conclusion, the various EBL spectral models exhibit a minor impact on the low-redshift gamma-ray axionscope. Nevertheless, this effect is anticipated to become more pronounced in future higher energy gamma-ray observation experiments.

Acknowledgments

A   General photon-ALP conversions

Here we present the general photon-ALP conversions in the homogeneous magnetic field and the calculation of the photon-ALP conversion probability [58, 65]. The photon-ALP

system (A_1, A_2, and a) can be described by

$$\psi(x_3) = \begin{pmatrix} A_1(x_3) \\ A_2(x_3) \\ a(x_3) \end{pmatrix}, \tag{A.1}$$

where x_3 is the direction of propagation, A_1 and A_2 represent the linear polarization amplitudes of the photons in the perpendicular directions (x_1, x_2)

$$|A_1\rangle = \begin{pmatrix} 1 \\ 0 \\ 0 \end{pmatrix}, \quad |A_2\rangle = \begin{pmatrix} 0 \\ 1 \\ 0 \end{pmatrix}, \quad |a\rangle = \begin{pmatrix} 0 \\ 0 \\ 1 \end{pmatrix}. \tag{A.2}$$

Then the equation of motion for the photon-ALP system in the magnetic field can be described by

$$\left(i\frac{d}{dx_3} + E + \mathcal{M}(E, x_3) \right) \psi(x_3) = 0, \tag{A.3}$$

where E is the photon-ALP beam energy, and $\mathcal{M}(E, x_3)$ is the mixing matrix

$$\mathcal{M}(E, x_3) = \begin{pmatrix} \Delta_{11}(E, x_3) & \Delta_{12}(E, x_3) & \Delta_{a\gamma,1}(x_3) \\ \Delta_{21}(E, x_3) & \Delta_{22}(E, x_3) & \Delta_{a\gamma,2}(x_3) \\ \Delta_{a\gamma,1}(x_3) & \Delta_{a\gamma,2}(x_3) & \Delta_{aa}(E) \end{pmatrix}. \tag{A.4}$$

These terms are given by

$$\Delta_{11}(E, x_3) = \Delta_{\mathrm{pl}}(E, x_3) + 2\Delta_{\mathrm{QED}}(E, x_3) + \Delta_{\mathrm{CMB}}(E), \tag{A.5}$$

$$\Delta_{22}(E, x_3) = \Delta_{\mathrm{pl}}(E, x_3) + \frac{7}{2}\Delta_{\mathrm{QED}}(E, x_3) + \Delta_{\mathrm{CMB}}(E), \tag{A.6}$$

with

$$\Delta_{\mathrm{pl}}(E, x_3) = -\frac{\omega_{\mathrm{pl}}^2(x_3)}{2E} \simeq -1.08 \times 10^{-1} \left(\frac{n_e}{\mathrm{cm}^{-3}}\right) \left(\frac{E}{1\,\mathrm{GeV}}\right)^{-1} \mathrm{Mpc}^{-1}, \tag{A.7}$$

$$\Delta_{\mathrm{QED}}(E, x_3) = \frac{\alpha E}{45\pi} \left(\frac{B_T(x_3)}{B_{\mathrm{cr}}}\right)^2 \simeq 4.10 \times 10^{-12} \left(\frac{E}{1\,\mathrm{GeV}}\right) \left(\frac{B_T(x_3)}{1\,\mathrm{nG}}\right)^2 \mathrm{Mpc}^{-1}, \tag{A.8}$$

$$\Delta_{\mathrm{CMB}}(E) = \rho_{\mathrm{CMB}}E \simeq 0.80 \times 10^{-4} \left(\frac{E}{1\,\mathrm{GeV}}\right) \mathrm{Mpc}^{-1}, \tag{A.9}$$

$$\Delta_{a\gamma}(x_3) = \frac{1}{2}g_{a\gamma}B_T(x_3) \simeq 1.52 \times 10^{-2} \left(\frac{g_{a\gamma}}{10^{-11}\,\mathrm{GeV}^{-1}}\right) \left(\frac{B_T(x_3)}{1\,\mathrm{nG}}\right) \mathrm{Mpc}^{-1}, \tag{A.10}$$

$$\Delta_{aa}(E) = -\frac{m_a^2}{2E} \simeq -0.78 \times 10^2 \left(\frac{m_a}{10^{-9}\,\mathrm{GeV}}\right)^2 \left(\frac{E}{1\,\mathrm{GeV}}\right)^{-1} \mathrm{Mpc}^{-1}. \tag{A.11}$$

Note that the Faraday rotation terms $\Delta_{12}(E, x_3)$ and $\Delta_{21}(E, x_3)$ can be neglected. Here the term $\Delta_{\mathrm{pl}}(E, x_3)$ represents the plasma effect when the photon-ALP system propagates in the plasma environment with the plasma frequency

$$\omega_{\mathrm{pl}} = \sqrt{\frac{4\pi\alpha n_e}{m_e}}, \tag{A.12}$$

where α is the fine-structure constant, n_e and m_e are the free electron number density and mass, respectively. The term $\Delta_{\mathrm{QED}}(E, x_3)$ represents the QED vacuum polarization effect with the critical magnetic field [66]

$$B_{\mathrm{cr}} = \frac{m_e^2}{|e|} \simeq 4.41 \times 10^{13}\,\mathrm{G}\,, \tag{A.13}$$

and the term $\Delta_{\mathrm{CMB}}(E, x_3)$ represents the CMB photon dispersion effect with [67]

$$\rho_{\mathrm{CMB}} \simeq 0.511 \times 10^{-42}\,. \tag{A.14}$$

If considering the transversal magnetic field B_T is aligned along the direction x_2, the mixing matrix $\mathcal{M}(E, x_3)$ can be rewriten as

$$\mathcal{M}(E, x_3) = \begin{pmatrix} \Delta_{11}(E, x_3) & 0 & 0 \\ 0 & \Delta_{22}(E, x_3) & \Delta_{a\gamma}(x_3) \\ 0 & \Delta_{a\gamma}(x_3) & \Delta_{aa}(E) \end{pmatrix}. \tag{A.15}$$

Finally, the photon-ALP conversion probability in the homogeneous magnetic field can be described by

$$\mathcal{P}_{a\gamma}(E, x_3) = \left(\frac{g_{a\gamma} B_T L_{\mathrm{osc}}(E)}{2\pi} \right)^2 \sin^2 \left(\frac{\pi x_3}{L_{\mathrm{osc}}(E)} \right)\,, \tag{A.16}$$

where $L_{\mathrm{osc}}(E)$ is the oscillation length

$$\begin{aligned} L_{\mathrm{osc}}(E) &= 2\pi \left[(\Delta_{22}(E) - \Delta_{aa}(E))^2 + 4\Delta_{a\gamma}^2 \right]^{-1/2} \\ &= 2\pi \left[\left[\frac{|m_a^2 - \omega_{\mathrm{pl}}^2|}{2E} + E \left(\frac{7\alpha}{90\pi} \left(\frac{B_T}{B_{\mathrm{cr}}} \right)^2 + \rho_{\mathrm{CMB}} \right) \right]^2 + g_{a\gamma}^2 B_T^2 \right]^{-1/2}. \end{aligned} \tag{A.17}$$

References

[1] R. Peccei and H. R. Quinn, *CP Conservation in the Presence of Instantons*, *Phys. Rev. Lett.* **38** (1977) 1440–1443.

[2] R. Peccei and H. R. Quinn, *Constraints Imposed by CP Conservation in the Presence of Instantons*, *Phys. Rev. D* **16** (1977) 1791–1797.

[3] S. Weinberg, *A New Light Boson?*, *Phys. Rev. Lett.* **40** (1978) 223–226.

[4] F. Wilczek, *Problem of Strong P and T Invariance in the Presence of Instantons*, *Phys. Rev. Lett.* **40** (1978) 279–282.

[5] J. Preskill, M. B. Wise and F. Wilczek, *Cosmology of the Invisible Axion*, *Phys. Lett. B* **120** (1983) 127–132.

[6] L. Abbott and P. Sikivie, *A Cosmological Bound on the Invisible Axion*, *Phys. Lett. B* **120** (1983) 133–136.

[7] M. Dine and W. Fischler, *The Not So Harmless Axion*, *Phys. Lett. B* **120** (1983) 137–141.

[8] A. Arvanitaki, S. Dimopoulos, S. Dubovsky, N. Kaloper and J. March-Russell, *String Axiverse*, *Phys. Rev. D* **81** (2010) 123530, [`0905.4720`].

[9] P. Svrcek and E. Witten, *Axions In String Theory*, *JHEP* **06** (2006) 051, [`hep-th/0605206`].

[10] D. Cadamuro and J. Redondo, *Cosmological bounds on pseudo Nambu-Goldstone bosons*, *JCAP* **02** (2012) 032, [`1110.2895`].

[11] P. Arias, D. Cadamuro, M. Goodsell, J. Jaeckel, J. Redondo and A. Ringwald, *WISPy Cold Dark Matter*, *JCAP* **06** (2012) 013, [`1201.5902`].

[12] W. Chao, M. Jin, H.-J. Li, Y.-Q. Peng and Y. Wang, *Axionlike dark matter from the type-II seesaw mechanism*, *Phys. Rev. D* **109** (2024) 115027, [`2210.13233`].

[13] C. O'HARE, *cajohare/axionlimits: Axionlimits*, July, 2020. 10.5281/zenodo.3932430.

[14] A. Mirizzi, G. G. Raffelt and P. D. Serpico, *Signatures of Axion-Like Particles in the Spectra of TeV Gamma-Ray Sources*, *Phys. Rev. D* **76** (2007) 023001, [`0704.3044`].

[15] M. Simet, D. Hooper and P. D. Serpico, *The Milky Way as a Kiloparsec-Scale Axionscope*, *Phys. Rev. D* **77** (2008) 063001, [`0712.2825`].

[16] D. Hooper and P. D. Serpico, *Detecting Axion-Like Particles With Gamma Ray Telescopes*, *Phys. Rev. Lett.* **99** (2007) 231102, [`0706.3203`].

[17] H.E.S.S. collaboration, F. Aharonian et al., *New constraints on the Mid-IR EBL from the HESS discovery of VHE gamma rays from 1ES 0229+200*, *Astron. Astrophys.* **475** (2007) L9–L13, [`0709.4584`].

[18] MAGIC collaboration, E. Aliu et al., *Very-High-Energy Gamma Rays from a Distant Quasar: How Transparent Is the Universe?*, *Science* **320** (2008) 1752, [`0807.2822`].

[19] H.E.S.S. collaboration, A. Abramowski et al., *Constraints on axionlike particles with H.E.S.S. from the irregularity of the PKS 2155-304 energy spectrum*, *Phys. Rev. D* **88** (2013) 102003, [`1311.3148`].

[20] FERMI-LAT collaboration, M. Ajello et al., *Search for Spectral Irregularities due to Photon–Axionlike-Particle Oscillations with the Fermi Large Area Telescope*, *Phys. Rev. Lett.* **116** (2016) 161101, [`1603.06978`].

[21] K. Kohri and H. Kodama, *Axion-Like Particles and Recent Observations of the Cosmic Infrared Background Radiation*, *Phys. Rev. D* **96** (2017) 051701, [`1704.05189`].

[22] C. Zhang, Y.-F. Liang, S. Li, N.-H. Liao, L. Feng, Q. Yuan et al., *New bounds on axionlike particles from the Fermi Large Area Telescope observation of PKS 2155-304*, *Phys. Rev. D* **97** (2018) 063009, [`1802.08420`].

[23] M. M. Ivanov, Y. Y. Kovalev, M. L. Lister, A. G. Panin, A. B. Pushkarev, T. Savolainen et al., *Constraining the photon coupling of ultra-light dark-matter axion-like particles by polarization variations of parsec-scale jets in active galaxies*, *JCAP* **02** (2019) 059, [`1811.10997`].

[24] Y.-F. Liang, C. Zhang, Z.-Q. Xia, L. Feng, Q. Yuan and Y.-Z. Fan, *Constraints on axion-like particle properties with TeV gamma-ray observations of Galactic sources*, *JCAP* **06** (2019) 042, [`1804.07186`].

[25] M. Libanov and S. Troitsky, *On the impact of magnetic-field models in galaxy clusters on constraints on axion-like particles from the lack of irregularities in high-energy spectra of astrophysical sources*, *Phys. Lett. B* **802** (2020) 135252, [`1908.03084`].

[26] G. Long, W. Lin, P. Tam and W. Zhu, *Testing the CIBER cosmic infrared background measurements and axionlike particles with observations of TeV blazars*, *Phys. Rev. D* **101** (2020) 063004, [1912.05309].

[27] J. Guo, H.-J. Li, X.-J. Bi, S.-J. Lin and P.-F. Yin, *The implications of the axion like particle from the Fermi-LAT and H.E.S.S. observations of PG 1553+113 and PKS 2155-304*, *Chin. Phys. C* **45** (2021) 025105, [2002.07571].

[28] X.-J. Bi, Y. Gao, J. Guo, N. Houston, T. Li, F. Xu et al., *Axion and dark photon limits from Crab Nebula high energy gamma-rays*, *Phys. Rev. D* **103** (2021) 043018, [2002.01796].

[29] H.-J. Li, J.-G. Guo, X.-J. Bi, S.-J. Lin and P.-F. Yin, *Limits on axion-like particles from Mrk 421 with 4.5-year period observations by ARGO-YBJ and Fermi-LAT*, *Phys. Rev. D* **103** (2021) 083003, [2008.09464].

[30] J.-G. Cheng, Y.-J. He, Y.-F. Liang, R.-J. Lu and E.-W. Liang, *Revisiting the analysis of axion-like particles with the Fermi-LAT gamma-ray observation of NGC1275*, *Phys. Lett. B* **821** (2021) 136611, [2010.12396].

[31] H.-J. Li, X.-J. Bi and P.-F. Yin, *Searching for axion-like particles with the blazar observations of MAGIC and Fermi-LAT **, *Chin. Phys. C* **46** (2022) 085105, [2110.13636].

[32] H.-J. Li, *Relevance of VHE blazar spectra models with axion-like particles*, *JCAP* **02** (2022) 025, [2112.14145].

[33] C. Dessert, D. Dunsky and B. R. Safdi, *Upper limit on the axion-photon coupling from magnetic white dwarf polarization*, *Phys. Rev. D* **105** (2022) 103034, [2203.04319].

[34] H.-J. Li, *Probing photon-ALP oscillations from the flat spectrum radio quasar 4C+21.35*, *Phys. Lett. B* **829** (2022) 137047, [2203.08573].

[35] S. Jacobsen, T. Linden and K. Freese, *Constraining axion-like particles with HAWC observations of TeV blazars*, *JCAP* **10** (2023) 009, [2203.04332].

[36] L. Mastrototaro, P. Carenza, M. Chianese, D. F. G. Fiorillo, G. Miele, A. Mirizzi et al., *Constraining axion-like particles with the diffuse gamma-ray flux measured by the Large High Altitude Air Shower Observatory*, *Eur. Phys. J. C* **82** (2022) 1012, [2206.08945].

[37] H.-J. Li, *Primordial black holes induced stochastic axion-photon oscillations in primordial magnetic field*, *JCAP* **11** (2022) 045, [2208.04605].

[38] D. Noordhuis, A. Prabhu, S. J. Witte, A. Y. Chen, F. Cruz and C. Weniger, *Novel Constraints on Axions Produced in Pulsar Polar-Cap Cascades*, *Phys. Rev. Lett.* **131** (2023) 111004, [2209.09917].

[39] B. P. Pant, Sunanda, R. Moharana and S. S., *Implications of photon-ALP oscillations in the extragalactic neutrino source TXS 0506+056 at sub-PeV energies*, *Phys. Rev. D* **108** (2023) 023016, [2210.12652].

[40] L.-Q. Gao, X.-J. Bi, J.-G. Guo, W. Lin and P.-F. Yin, *Constraints on axionlike particles from observations of Mrk 421 using the CLs method*, *Phys. Rev. D* **109** (2024) 063003, [2309.02166].

[41] B. P. Pant, *Probing photon-ALP oscillations from the MAGIC observations of FSRQ QSO B1420+326*, *Phys. Rev. D* **109** (2024) 023011, [2310.16634].

[42] H.-J. Li, W. Chao and Y.-F. Zhou, *Axion limits from the 10-year gamma-ray emission 1ES 1215+303*, *Phys. Lett. B* **850** (2024) 138531, [2312.05555].

[43] J. Li, X.-J. Bi, L.-Q. Gao, X. Huang, R.-M. Yao and P.-F. Yin, *Constraints on axion-like particles from the observation of Galactic sources by the LHAASO**, *Chin. Phys. C* **48** (2024) 065107, [2401.01829].

[44] W.-Q. Guo, Z.-Q. Xia and X. Huang, *Constraining axion-like particles dark matter in Coma Berenices with FAST*, *Phys. Lett. B* **852** (2024) 138631, [2404.04881].

[45] J. Ruz et al., *NuSTAR as an Axion Helioscope*, 2407.03828.

[46] S. Porras-Bedmar, M. Meyer and D. Horns, *Novel bounds on decaying axion-like-particle dark matter from the cosmic background*, 2407.10618.

[47] L.-Q. Gao, X.-J. Bi, J. Li and P.-F. Yin, *Impact of Parameters in the Blazar Jet Magnetic Field Model on Axion-Like Particle Constraints*, 2407.20118.

[48] B. Betancourt Kamenetskaia, N. Fraija and G. Herrera, *Polarization Measurements as a Probe of Axion-Photon Coupling: a Study of GRB 221009A*, 2408.07352.

[49] B.-Y. Zhu, X. Huang and P.-F. Yin, *Constraints on Axion-like Particles from the gamma-ray observation of the Galactic Center*, 2408.12234.

[50] H.-J. Li and W. Chao, *Axion effects on gamma-ray spectral irregularities with AGN redshift uncertainty*, *Phys. Rev. D* **107** (2023) 063031, [2211.00524].

[51] HAWC collaboration, A. Albert et al., *Long-term Spectra of the Blazars Mrk 421 and Mrk 501 at TeV Energies Seen by HAWC*, *Astrophys. J.* **929** (2022) 125, [2106.03946].

[52] H.-J. Li, W. Chao and Y.-F. Zhou, *Upper limit on the axion-photon coupling from Markarian 421*, *Phys. Lett. B* **858** (2024) 139075, [2406.00387].

[53] A. Franceschini, G. Rodighiero and M. Vaccari, *The extragalactic optical-infrared background radiations, their time evolution and the cosmic photon-photon opacity*, *Astron. Astrophys.* **487** (2008) 837, [0805.1841].

[54] PARTICLE DATA GROUP collaboration, S. Navas et al., *Review of particle physics*, *Phys. Rev. D* **110** (2024) 030001.

[55] J. D. Finke, S. Razzaque and C. D. Dermer, *Modeling the Extragalactic Background Light from Stars and Dust*, *Astrophys. J.* **712** (2010) 238–249, [0905.1115].

[56] R. C. Gilmore, R. S. Somerville, J. R. Primack and A. Dominguez, *Semi-analytic modeling of the EBL and consequences for extragalactic gamma-ray spectra*, *Mon. Not. Roy. Astron. Soc.* **422** (2012) 3189, [1104.0671].

[57] A. Dominguez et al., *Extragalactic Background Light Inferred from AEGIS Galaxy SED-type Fractions*, *Mon. Not. Roy. Astron. Soc.* **410** (2011) 2556, [1007.1459].

[58] A. De Angelis, G. Galanti and M. Roncadelli, *Relevance of axion-like particles for very-high-energy astrophysics*, *Phys. Rev. D* **84** (2011) 105030, [1106.1132]. [Erratum: Phys.Rev.D 87, 109903 (2013)].

[59] PLANCK collaboration, P. Ade et al., *Planck 2015 results. XIX. Constraints on primordial magnetic fields*, *Astron. Astrophys.* **594** (2016) A19, [1502.01594].

[60] M. Pshirkov, P. Tinyakov and F. Urban, *New limits on extragalactic magnetic fields from rotation measures*, *Phys. Rev. Lett.* **116** (2016) 191302, [1504.06546].

[61] R. Jansson and G. R. Farrar, *A New Model of the Galactic Magnetic Field*, *Astrophys. J.* **757** (2012) 14, [1204.3662].

[62] R. Jansson and G. R. Farrar, *The Galactic Magnetic Field*, *Astrophys. J. Lett.* **761** (2012) L11, [1210.7820].

[63] PLANCK collaboration, R. Adam et al., *Planck intermediate results.: XLII. Large-scale Galactic magnetic fields*, *Astron. Astrophys.* **596** (2016) A103, [1601.00546].

[64] M. Unger and G. R. Farrar, *Uncertainties in the Magnetic Field of the Milky Way*, 7, 2017. 1707.02339.

[65] G. Raffelt and L. Stodolsky, *Mixing of the Photon with Low Mass Particles*, *Phys. Rev. D* **37** (1988) 1237.

[66] J. S. Schwinger, *On gauge invariance and vacuum polarization*, *Phys. Rev.* **82** (1951) 664–679.

[67] A. Dobrynina, A. Kartavtsev and G. Raffelt, *Photon-photon dispersion of TeV gamma rays and its role for photon-ALP conversion*, *Phys. Rev. D* **91** (2015) 083003, [1412.4777]. [Erratum: Phys.Rev.D 95, 109905 (2017)].